

Phosphorus burial in ferruginous SiO₂-rich Mesoproterozoic sediments

Brooke R. Johnson, Rosalie Tostevin*, Philip Gopon, Jon Wells, Stuart A. Robinson and Nicholas J. Tosca

Department of Earth Sciences, University of Oxford, South Parks Road, Oxford OX1 3AN, UK

ABSTRACT

Persistently low atmospheric oxygen requires that net organic carbon burial was muted through much of Earth's middle age. In order to achieve global mass balance with respect to O₂, recent models have suggested that redox-dependent mechanisms, such as Fe(II)-phosphate precipitation, limited phosphate availability in dominantly anoxic and ferruginous oceans, in turn limiting net primary production, and therefore organic carbon burial. Nevertheless, observational constraints on phosphorus cycling in ferruginous Proterozoic systems are rare, leaving these models largely untested. Here, we present high-resolution petrographic and mineralogical data showing that the 1.3 Ga Sherwin Ironstone (Roper Group, Australia) was dominated by syndepositional precipitation of the Fe(II)-silicate minerals greenalite and berthierine, interlaminated with abundant authigenic calcium fluorapatite (CFA). Set in a quantitative geochemical framework, these data reveal that elevated marine SiO_{2(aq)} concentrations facilitated extensive Fe(II)-silicate production, leaving CFA, rather than Fe(II)-phosphate, as the principal inorganic phosphorous sink in shallow-water Roper Group sediments. More broadly, the physical and chemical factors that triggered Fe(II)-silicate and CFA burial in the Roper Seaway highlight semi-restricted basins as important loci of phosphorus removal from the mid-Proterozoic ocean.

INTRODUCTION

Low atmospheric oxygen is considered a defining characteristic of the Precambrian Earth, and recent models have highlighted the biogeochemical implications of a stable low-oxygen world. In order to stabilize low atmospheric O₂, some models hypothesize that the rate of net primary production (NPP) must have been lower (up to 10×–100×) than at present, reducing organic carbon burial (Derry, 2015; Laakso and Schrag, 2018a). Phosphorus limitation has emerged as the most likely mechanism to have attenuated NPP (Laakso and Schrag, 2018a, 2018b) and organic carbon burial. Several hypotheses have focused on redox-dependent mechanisms that might have limited P availability in anoxic and ferruginous oceans (Laakso and Schrag, 2014; Derry, 2015). Recently, a compilation of the total phosphorous concentration ([P]) in shales has revealed a four-fold increase that began in the early to mid-Neopro-

terozoic, continuing to modern times (Reinhard et al., 2017). This record is thought to reflect a major shift from redox-dependent P limitation to widespread P availability in the water column with the demise of Fe-rich waters (Reinhard et al., 2017).

However, direct observations that constrain P cycling in ferruginous Proterozoic systems are rare. For example, low [P] in many mid-Proterozoic shales has been interpreted to reflect P limitation through Fe(II)-phosphate precipitation in ferruginous systems (Derry, 2015), P scavenging through green rust precipitation (Zegeye et al., 2012), and adsorption and/or coprecipitation with Fe(III)-oxides (Jones et al., 2015). Although these mechanisms receive support from environmental analogues and geochemical models, they have not been tested against detailed mineralogical and sedimentological data from Proterozoic rocks. In addition, the stratigraphic distribution of syndepositional and early diagenetic chert in Proterozoic rocks reflects a marine system characterized by elevated SiO_{2(aq)} concentrations (Maliva et al., 2005), yet silica does not feature in current models or analogues for the mid-Proterozoic P cycle.

Here, to investigate the role of ferruginous and SiO₂-rich conditions on phosphate cycling in shallow-marine environments, we conducted a high-resolution sedimentological, mineralogical, and geochemical study of the 1.3 Ga Sherwin Ironstone of the Roper Superbasin, Northern Territory, Australia. The Sherwin Ironstone records an episode of Fe-rich chemical sedimentation in the Mesoproterozoic, offering a valuable window into contemporaneous Fe and P cycling.

GEOLOGICAL BACKGROUND AND METHODS

The Roper Superbasin hosts an exceptionally well-preserved record of sedimentation across multiple epicratonic basins of northern Australia (Munson, 2016). Sediment fill is packaged into six transgressive sequences of basinal shales and proximal sands, bound by intercycle erosional surfaces and ironstones (Munson, 2016). Local flexural tectonics controlled both relative sea level and sedimentation, whereby erosional loading of the basin caused subsidence in the depocenter (Abbott and Sweet, 2000; Munson, 2016).

Iron-rich chemical sediments are common across the Roper Superbasin as sequence-bounding ironstones and/or sandstones with Fe-rich cement, which were deposited during the initial stages of regional transgression (Abbott and Sweet, 2000). The most significant of these, the 1.3 Ga Sherwin Ironstone (Fig. 1; Yang et al., 2018), is dominated by iron-cemented sandstones and subordinate beds of Fe-silicate ooids and laminated Fe-silicate chemical sediment, reflecting shallow-marine upper-shoreface sedimentation (Cochrane and Edwards, 1960; Munson, 2016).

To examine chemical sedimentation associated with the Sherwin Ironstone, we logged and sampled six drill cores through the unit and examined 120 thin sections by optical microscopy and scanning electron microscopy–energy dispersive X-ray spectroscopy (SEM-EDS) using an FEI Quanta 650 FEG SEM. Subsamples of

*Current address: Department of Geological Sciences, University of Cape Town, Rondebosch, Cape Town 7701, South Africa.

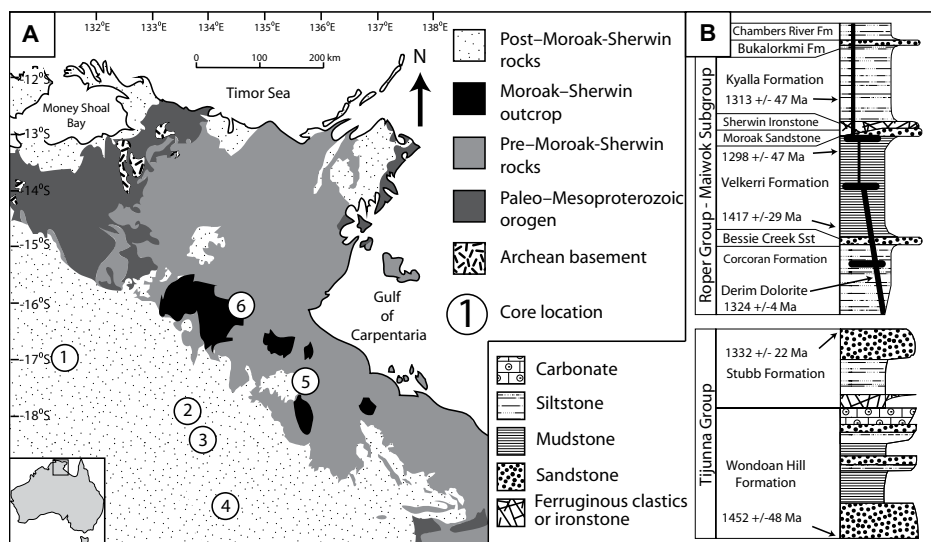


Figure 1. (A) Simplified geological map of the northernmost Northern Territory, Australia. Numbers denote approximate core locations: 1—99VRNTGSD2 (99VR); 2—McMannus-1a (MM1a); 3—Shenandoah-1a (SD1a); 4—12BC; 5—Scarborough 1 (Sc1); 6—Urapunga 4 (UP4) and Sherwin Ironstone Quarry (see the Data Repository [see footnote 1]). (B) Generalized stratigraphy of upper Roper and Tjunna Groups (from Munson, 2016; Yang et al., 2018). Sst—sandstone.

petrographic facies were microdrilled and analyzed for bulk and clay-specific mineralogy at the University of Oxford (Oxford, UK) using a Panalytical Empyrean Series 2 X-ray diffractometer (XRD) equipped with a Co K α source at 40 kV and 40 mA (see the GSA Data Repository¹).

¹GSA Data Repository item 2020031, age models, lithofacies details, extended methods, detailed discussion of vivianite formation, and additional data figures, is available online at <http://www.geosociety.org/datarepository/2020/>, or on request from editing@geosociety.org.

PRIMARY DEPOSITION OF Fe^{2+} SILICATES AND PHOSPHATE IN THE SHERWIN IRONSTONE

Petrographic and mineralogical data (Figs. 2 and 3) delineate three facies of chemical sediments: (1) laminated Fe-silicate-rich beds, (2) beds of Fe-silicate ooids with erosional surfaces and high-angle cross bedding, and (3) medium-to coarse-grained quartz sand cemented by various Fe minerals (Cochrane and Edwards, 1960). In all facies, authigenic berthierine and greenalite represent the principal building blocks of the Sherwin Ironstone (Fig. 2). The Sherwin

Ironstone was deposited in a range of high-energy shallow-water settings, from shoaling bars to upper shoreface, as indicated by abundant shallow-water sedimentary features (Cochrane and Edwards, 1960; Munson, 2016). Recent experimental work has shown that greenalite precipitation occurs under fully anoxic and ferruginous conditions (Tosca et al., 2016). Unlike berthierine (an Fe(II)- and Al-bearing silicate), the formation of which requires pore-water Fe^{2+} and preexisting aluminosilicate minerals (Bhattacharyya, 1983), the near absence of Al in the greenalite structure facilitates nucleation from the water column (Tosca et al., 2016; Fig. DR7 in the Data Repository). Thus, ferruginous waters commonly expanded onto the shallow shelf in the Roper Superbasin.

Powder XRD and SEM-EDS (Figs. 2 and 3) indicate that calcium fluorapatite (CFA) is an important constituent of the Sherwin Ironstone. CFA occurs as aggregates of anhedral grains within authigenic Fe-silicate cements, as well as within Fe-silicate ooid laminae (Figs. 2 and 3). In both cases, textural relationships indicate that CFA precipitated along with Fe-silicates (Fig. 3). CFA within Fe-silicate ooids (Fig. 3) indents underlying Fe-silicate lamina, indicating that the ooid was plastic when the CFA adhered to its outer surface. Further deformation probably occurred during reworking of the ooids, as indicated by their spastolitic texture. These petrographic relationships indicate that both Fe-silicates and CFA are primary precipitates. Detrital apatite in the Sherwin Ironstone can be distinguished based on its tabular habit, enrichment in Ca and rare earth elements, and lack of detectable F. Our petrographic observations also indicate that most Fe-oxides present

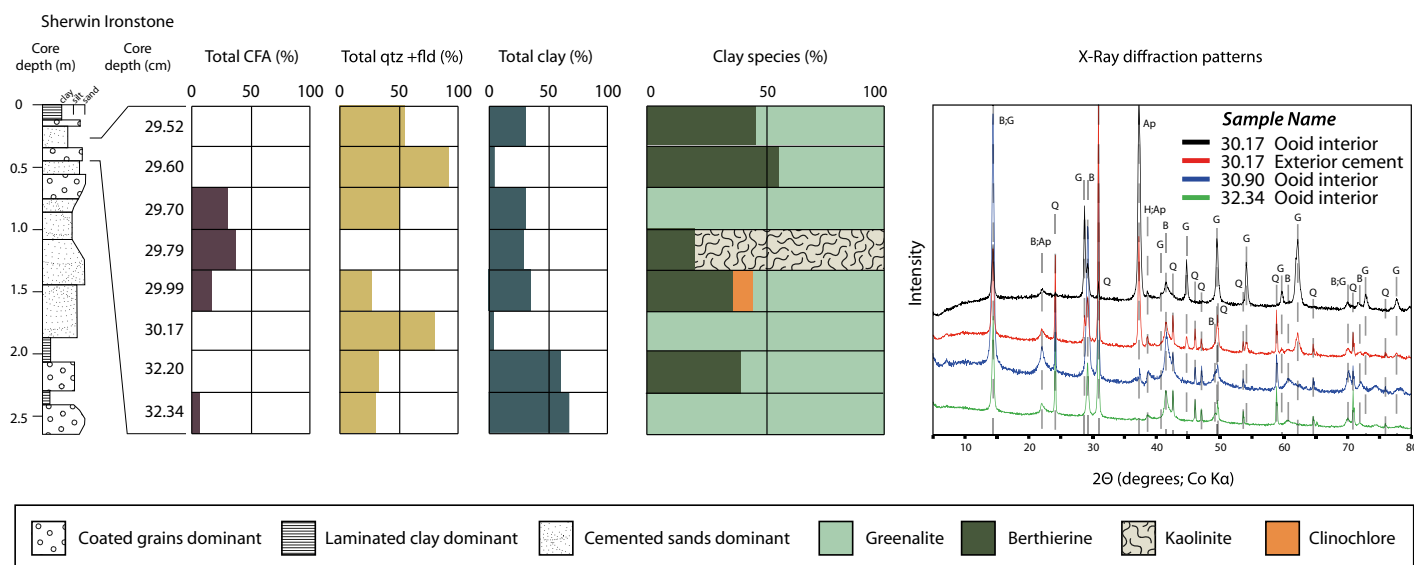


Figure 2. Simplified graphic log of Sherwin Ironstone from core Urapunga 4 (UP4), Northern Territory, Australia (left; Fig. 1); associated X-ray diffraction (XRD) results from microdrilled authigenic cements and coated grains from interval 29.52–32.34 cm (center); and typical XRD profiles of powders microdrilled from ferruginous ooids of the Sherwin Ironstone (right), dominated by varying abundances of quartz (Q), berthierine (B), greenalite (G), and carbonate fluorapatite (Ap). Trace amounts of hematite (H) are present in samples. CFA—calcium fluorapatite; Qtz—quartz; Fld—feldspar.

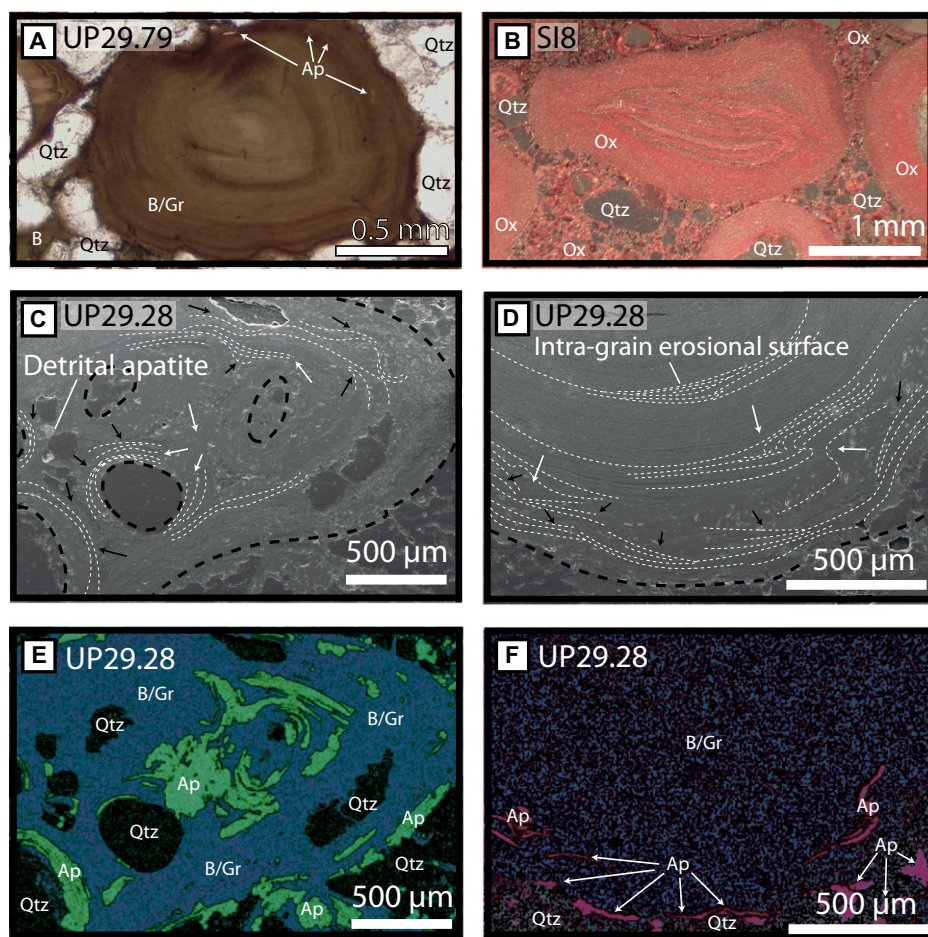


Figure 3. Coated grains from Sherwin Ironstone (Northern Territory, Australia); sample names in top left. (A) Pristine greenalite-berthierine coated grains in plane-polarized light. **(B)** Ooid from surface quarry in reflected light. Ooid has undergone complete oxidation to hematite and goethite. Quartz sand matrix now contains hematite and silica cement. **(C,D)** Scanning electron microscopy–backscatter electron maps with key features highlighted: black dashes, grain boundary and nucleus; white dashes, primary internal lamina; black arrows, onlap and infill of lamina over apatite grains; white arrows, displacement of lamina by adhesion and continued growth of apatite grains. **(E,F)** Energy dispersive X-ray spectroscopy element maps for phosphorus (green in E, pink in F), Fe (light blue in E, dark blue in F) and Si (dark green in E, gray in F). Note the negative correlation between P and Fe. Abbreviations: B/Gr—berthierine and greenalite; Ap—calcium fluorapatite; Qtz—quartz; Ox—iron oxide. A and C–F were taken from core Urupunga 4 (UP4); B is from the surface quarry. See Figure 1 and the Data Repository (see footnote 1) for geographic locations.

within the Sherwin Ironstone are the products of late-stage alteration (Fig. 3B; Cochrane and Edwards, 1960; Data Repository).

DISCUSSION AND CONCLUSIONS

Together, petrographic and mineralogical constraints indicate that CFA was deposited with Fe(II)-silicates of the Sherwin Ironstone at or just below the seafloor (Figs. 3A, 3C, and 3D; Fig. DR6). Although these data do not rule out the possibility that some of the PO_4 in CFA minerals was derived through dissolution of Fe-oxides, they support the inference that the high aqueous PO_4 concentrations necessary for CFA nucleation extended above the sediment–water interface. In addition, the decoupling between detrital mineral phases and CFA suggests that aqueous PO_4 accumulation was not strongly

linked to input derived from riverine sources (Fig. 2). Similarly, while organic-matter diagenesis would be expected to have released PO_4 and fuel CFA precipitation (i.e., an expression of a process known as “sink-switching”; Ruttenberg and Berner, 1993), the Sherwin Ironstone is conspicuously organic poor, with total organic carbon <0.1 wt% (data not shown). Relatively high PO_4 concentrations in the water column could also be due to recycling of organic matter derived from primary production (i.e., Lenton and Daines, 2018; Poulton, 2017) or a limited supply of fixed nitrogen (i.e., Sanchez-Baracaldo et al., 2014; Koehler et al., 2017).

Regardless of how PO_4 accumulated in the water column during Sherwin Ironstone deposition, our data demonstrate that CFA was an important terminal P sink during Roper Group

chemical sedimentation, precipitating contemporaneously with Fe(II)-silicates from a ferruginous water column. Available constraints on apatite and greenalite formation pathways define the chemical solution space required to stabilize these two minerals in Roper Group sediments. Once a specific combination of pH, $[\text{SiO}_2]$, and $[\text{Fe}^{2+}]$ is crossed, then an Fe(II)-silicate gel precipitates, and eventually reorders to form greenalite (Tosca et al., 2016). Assuming saturation with respect to amorphous silica (supported by shallow-water chert deposition in proximally equivalent sediments), minimum $[\text{Fe}^{2+}]$ at greenalite nucleation may be determined across a range in pH from 7.2 [below which Fe(II)-silicate precipitation is too slow to occur over reasonable diagenetic time scales; Tosca et al., 2016] to 8.2, a reasonable upper limit based on current constraints on Proterozoic pH (Halevy and Bachan, 2017). Both experimental and observational evidence support an apatite formation pathway that first involves the nucleation of octacalcium phosphate, then subsequent recrystallization to apatite (Jahnke et al., 1982; Gunnars et al., 2004; Van Cappellen and Berner, 1991). Thus, a conservative upper limit for total $[\text{PO}_4]$ may be determined across the same pH window if marine $[\text{Ca}^{2+}]$ is known. Although few constraints on Mesoproterozoic marine $[\text{Ca}^{2+}]$ are available, 2.5 mmol/kg serves as a reasonable minimum, below which Ca-sulfate would not precipitate upon evaporation (inconsistent with Roper Superbasin and other Mesoproterozoic sediments; Grotzinger and Kasting, 1993). An upper limit of 30 mmol/kg $[\text{Ca}^{2+}]$ serves as a maximum based on Ca-isotope constraints of marine evaporites of the ca. 2.0 Ga Tulomozero Formation (northwestern Russia), and from evaporite geochemistry of the ca. 1200 Ma Society Cliffs Formation (northern Baffin Island, Canada) which indicates that $[\text{Ca}^{2+}]$, $[\text{K}^+]$, and $[\text{Na}^+]$ were close to modern values (Kah et al., 2001; Blättler et al., 2018). Combining these constraints yields the saturation state of Roper Superbasin water relative to vivianite, a common Fe(II)-phosphate mineral known to precipitate in modern marine and lacustrine sediments (more readily than the Mg-rich end members bobierite and baricite; Egger et al., 2015; Dijkstra et al., 2016; Fig. 4). These calculations show that for all conditions except those associated with alkaline pH and very high marine $[\text{Ca}^{2+}]$, the contemporaneous precipitation of greenalite and Ca-phosphate occurred despite significant vivianite supersaturation.

This combination of petrographic and mineralogical data with geochemical constraints reveals a significant kinetic barrier associated with vivianite precipitation, a conclusion reinforced by pore-water data from modern sediments. For example, a number of studies have reported significant supersaturation with respect to Fe(II)-phosphate in lacustrine, estuarine, and marine

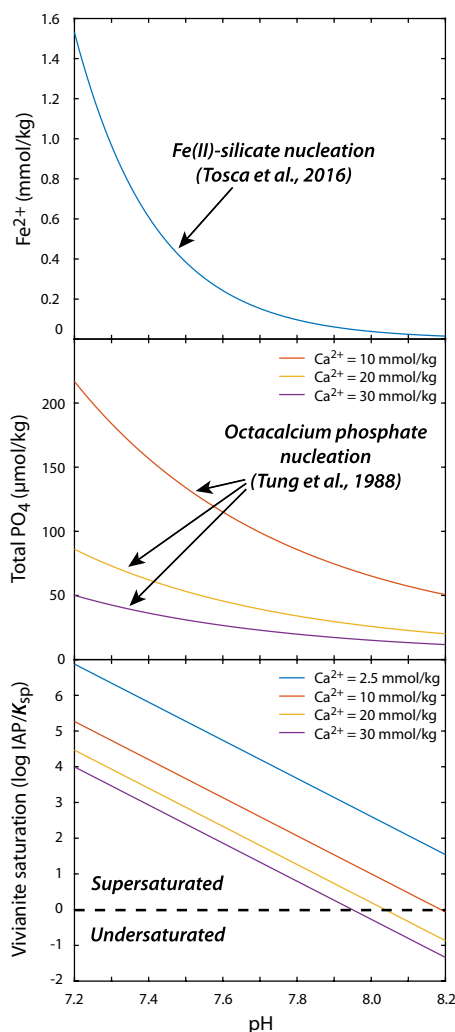


Figure 4. Chemical requirements for contemporaneous Fe(II)-silicate and Ca-phosphate nucleation at 25 °C, which together result in Fe(II)-phosphate supersaturation. The apparent solubility product for Fe(II)-silicate precursor and subsequent greenalite nucleation are from Tosca et al. (2016). Total PO₄ concentrations correspond to solubility of octacalcium phosphate, demonstrated as the initial precursor phase to apatite precipitation; solubility product is from Tung et al. (1988). Resulting supersaturation is with respect to vivianite, a common Fe(II)-phosphate (K_{sp} from Al-Borno and Tomson, 1994). IAP—ion activation product.

systems, despite the presence or absence of solid Fe(II)-phosphate phases (Postma, 1981; Rothe et al., 2016). This further indicates that when the threshold for nucleation has been reached in some diagenetic systems, Fe(II)-phosphate minerals may not grow rapidly enough to buffer PO₄ to equilibrium solubility levels. This kinetic limitation implies that Fe(II)-phosphate precipitation should occur in sedimentary environments that are routinely associated with excessive supersaturation. In fact, a number of recent studies have shown that modern marine Fe(II)-phosphate precipitation is dominantly confined to

sedimentary environments below the sulfate-methane transition zone (SMTZ; Egger et al., 2015; Dijkstra et al., 2016; März et al., 2018).

One significant difference between modern sedimentary environments conducive to Fe(II)-phosphate nucleation and the Sherwin Ironstone is the absence of other Fe(II)-bearing phases that kinetically compete for Fe²⁺. Indeed, at the Fe²⁺ concentrations and alkalinities associated with modern sediments below the SMTZ, very low SiO_{2(aq)} concentration typically precludes Fe(II)-silicate formation. However, in Proterozoic marine systems where SiO_{2(aq)} was much higher than in the modern ocean (Maliva et al., 2005), experimental constraints indicate that high [Fe²⁺] and alkalinities [and thus Fe(II)-phosphate supersaturation] may not have been reached without rapid nucleation of Fe(II)-silicates such as greenalite (Tosca et al., 2016). As our data indicate, the presence of elevated SiO_{2(aq)} in mid-Proterozoic marine systems appears to have efficiently sequestered Fe²⁺ in Fe(II)-silicate phases, while leaving CFA as the dominant inorganic sink for phosphorus.

Our conclusions receive additional support from a number of examples where Fe(II)-silicate minerals have precipitated in close association with Ca-phosphate; for instance, the Paleoproterozoic Sokoman Iron Formation of the Labrador Trough, eastern Canada (Pufahl et al., 2014), and Ordovician oolitic ironstones of Bell Island, Newfoundland, Canada (Todd et al., 2018). Oolitic ironstones composed of Fe-silicate and authigenic phosphates also occur in the early Jurassic Cleveland Ironstone, northern England, UK, in the Passwang Formation, Switzerland (Burkhalter, 1995; MacQuaker and Taylor, 1996), and in the Cretaceous of south-eastern Australia (Boyd et al., 2004).

Together, a variety of data indicate that elevated [SiO₂] and Fe(II)-silicate precipitation may have prevented Fe(II)-phosphate burial from Proterozoic seas, in contrast with models that envisage a link between PO₄ limitation and ferruginous chemistry (Planavsky et al., 2011; Derry, 2015; Reinhard et al., 2017). Nevertheless, the requirement for global oxygen mass balance implies that other mechanisms may have regulated marine PO₄ availability through the Proterozoic (Diaz et al., 2008; Cox et al., 2019). Our analyses also indicate that shallow epeiric seas such as the Roper Superbasin served as key depositional loci for both Fe(II)-silicates and Ca-phosphates. Unique physical and chemical factors, such as partial regional restriction coupled with enhanced alkalinity input from surrounding volcanic catchment (Cox et al., 2016), established these environments as permanent chemical sedimentary traps for both riverine and deep-marine (i.e., upwelling-derived) PO₄. This unusual set of geological conditions, apparently common in the mid-Proterozoic, would have impacted the global

marine PO₄ reservoir until the Tonian–Cryogenian breakup of Rodinia (Horton, 2015). A tectono-sedimentary influence on P burial also reconciles shale-hosted P and Fe-speciation records, which, when viewed together, suggest that Proterozoic P burial increased even though anoxic and/or ferruginous waters persisted well into the Paleozoic (Sperling et al., 2015). Nevertheless, further examination of Fe and P mineralogy preserved in ancient sediments will continue to reshape our understanding of Proterozoic biogeochemical cycling.

ACKNOWLEDGMENTS

We are grateful to Amber Jarret and Grant Cox for facilitating sample acquisition and helpful discussions. Staff at Geoscience Australia and the Northern Territory Geological Survey are thanked for provision of sample material and generous assistance with sample collection. Katherine Clayton collected the XRD data. Fatima Ali and Tobormory Mackay-Champion assisted with sample preparation and data collection, and Jon Wade assisted with acquiring SEM-EDS data. Steve Wyatt and Phil Holdship assisted with ICP-MS analysis. BRJ was funded by Natural Environment Research Council award NE/L002612/1. We thank Malcolm Wallace and two anonymous reviewers, whose thoughtful comments improved this manuscript.

REFERENCES CITED

- Abbott, S.T., and Sweet, I.P., 2000, Tectonic control on third-order sequences in a siliciclastic ramp-style basin: An example from the Roper Superbasin (Mesoproterozoic), northern Australia: *Australian Journal of Earth Sciences*, v. 47, p. 637–657, <https://doi.org/10.1046/j.1440-0952.2000.00795.x>.
- Al-Borno, A., and Tomson, M.B., 1994, The temperature dependence of the solubility product constant of vivianite: *Geochimica et Cosmochimica Acta*, v. 58, p. 5373–5378, [https://doi.org/10.1016/0016-7037\(94\)90236-4](https://doi.org/10.1016/0016-7037(94)90236-4).
- Bhattacharyya, D.P., 1983, Origin of berthierine in ironstones: *Clays and Clay Minerals*, v. 31, p. 173–182, <https://doi.org/10.1346/CCMN.1983.0310302>.
- Blättler, C.L., et al., 2018, Two-billion-year-old evaporites capture Earth's great oxidation: *Science*, v. 360, p. 320–323, <https://doi.org/10.1126/science.aar2687>.
- Boyd, G.A., Wallace, M.W., Holdgate, G.R., and Gallagher, S.J., 2004, Marine clays and porosity evolution in the Nullawarre Greensand, Otway Basin, southeastern Australia: Paper presented at Petroleum Exploration Society of Australia Eastern Australian Basin Symposium II, Adelaide, 19–22 September, p. 537–552.
- Burkhalter, R.M., 1995, Oolitic ironstones and ferruginous microbialites: Origin and relation to sequence stratigraphy (Aalenian and Bajocian, Swiss Jura mountains): *Sedimentology*, v. 42, p. 57–74, <https://doi.org/10.1111/j.1365-3091.1995.tb01271.x>.
- Cochrane, G.W., and Edwards, A.B., 1960, The Roper River Oolitic Ironstone Formations: Mineralogical Investigations, Technical Paper 1: Melbourne, Commonwealth Scientific and Industrial Research Organization, 28 p.
- Cox, G.M., Jarrett, A., Edwards, D., Crockford, P.W., Halverson, G.P., Collins, A.S., Poirier, A., and Li, Z.-X., 2016, Basin redox and primary productivity within the Mesoproterozoic Roper Seaway: *Chemical Geology*, v. 440, p. 101–114, <https://doi.org/10.1016/j.chemgeo.2016.06.025>.
- Cox, G.M., Sansjofre, P., Blades, M.L., Farkas, J., and Collins, A.S., 2019, Dynamic interaction between

- basin redox and the biogeochemical nitrogen cycle in an unconventional Proterozoic petroleum system: *Scientific Reports*, v. 9, 5200, <https://doi.org/10.1038/s41598-019-40783-4>.
- Derry, L.A., 2015, Causes and consequences of mid-Proterozoic anoxia: *Geophysical Research Letters*, v. 42, p. 8538–8546, <https://doi.org/10.1002/2015GL065333>.
- Diaz, R.J., Benitez-Nelson, C., Paterson, D., de Jonge, M.D., McNulty, I., and Brandes, J.A., 2008, Marine polyphosphate: A key player in geologic phosphorus sequestration: *Science*, v. 320, p. 652–655, <https://doi.org/10.1126/science.1151751>.
- Dijkstra, N., Slomp, C.P., Behrends, T., and Expedition 347 Scientists, 2016, Vivianite is a key sink for phosphorus in sediments of the Landsort Deep, an intermittently anoxic deep basin in the Baltic Sea: *Chemical Geology*, v. 438, p. 58–72, <https://doi.org/10.1016/j.chemgeo.2016.05.025>.
- Egger, M., Jilbert, T., Behrends, T., Rivard, C., and Slomp, C.P., 2015, Vivianite is a major sink for phosphorus in methanogenic coastal surface sediments: *Geochimica et Cosmochimica Acta*, v. 169, p. 217–235, <https://doi.org/10.1016/j.gca.2015.09.012>.
- Grotzinger, J.P., and Kasting, J.F., 1993, New constraints on Precambrian ocean composition: *The Journal of Geology*, v. 101, p. 235–243, <https://doi.org/10.1086/648218>.
- Gunnars, A., Blomqvist, S., and Martinsson, C., 2004, Inorganic formation of apatite in brackish seawater from the Baltic Sea: An experimental approach: *Marine Chemistry*, v. 91, p. 15–26, <https://doi.org/10.1016/j.marchem.2004.01.008>.
- Halevy, I., and Bachan, A., 2017, The geologic history of seawater pH: *Science*, v. 355, p. 1069–1071, <https://doi.org/10.1126/science.aal4151>.
- Horton, F., 2015, Did phosphorus derived from the weathering of large igneous provinces fertilize the Neoproterozoic ocean?: *Geochemistry Geophysics Geosystems*, v. 16, p. 1723–1738, <https://doi.org/10.1002/2015GC005792>.
- Jahnke, R.A., Emerson, S.R., Roe, K.K., and Burnett, W.C., 1982, The present day formation of apatite in Mexican continental margin sediments: *Geochimica et Cosmochimica Acta*, v. 47, p. 259–266, [https://doi.org/10.1016/0016-7037\(83\)90138-2](https://doi.org/10.1016/0016-7037(83)90138-2).
- Jones, C., Nomosatryo, S., Crowe, S.A., Bjerrum, C.J., and Canfield, D.E., 2015, Iron oxides, divalent cations, silica, and the early earth phosphorus crisis: *Geology*, v. 43, p. 135–138, <https://doi.org/10.1130/G36044.1>.
- Kah, L.C., Lyons, T.W., and Chesley, J.T., 2001, Geochemistry of a 1.2 Ga carbonate-evaporite succession, northern Baffin and Bylot Islands: Implications for Mesoproterozoic marine evolution: *Precambrian Research*, v. 111, p. 203–234, [https://doi.org/10.1016/S0301-9268\(01\)00161-9](https://doi.org/10.1016/S0301-9268(01)00161-9).
- Koehler, M.C., Stüeken, E.E., Kipp, M.A., Buick, R., and Knoll, A.H., 2017, Spatial and temporal trends in Precambrian nitrogen cycling: A Mesoproterozoic offshore nitrate minimum: *Geochimica et Cosmochimica Acta*, v. 198, p. 315–337, <https://doi.org/10.1016/j.gca.2016.10.050>.
- Laakso, T.A., and Schrag, D.P., 2014, Regulation of atmospheric oxygen during the Proterozoic: *Earth and Planetary Science Letters*, v. 388, p. 81–91, <https://doi.org/10.1016/j.epsl.2013.11.049>.
- Laakso, T.A., and Schrag, D.P., 2018a, A small marine biosphere in the Proterozoic: *Geobiology*, v. 17, p. 1–11, <https://doi.org/10.1111/gbi.12323>.
- Laakso, T.A., and Schrag, D.P., 2018b, Limitations on limitation: *Global Biogeochemical Cycles*, v. 32, p. 486–496, <https://doi.org/10.1002/2017GB005832>.
- Lenton, T.M., and Daines, S.J., 2018, The effects of marine eukaryote evolution on phosphorus, carbon and oxygen cycling across the Proterozoic–Phanerozoic transition: *Emerging Topics in Life Sciences*, v. 2, p. 267–278, <https://doi.org/10.1042/etls20170156>.
- MacQuaker, J.H.S., and Taylor, K.G., 1996, A sequence-stratigraphic interpretation of a mudstone-dominated succession: The Lower Jurassic Cleveland Ironstone Formation, UK: *Journal of the Geological Society*, v. 153, p. 759–770, <https://doi.org/10.1144/gsjgs.153.5.0759>.
- Maliva, R.G., Knoll, A.H., and Simonson, B.M., 2005, Secular change in the Precambrian silica cycle: Insights from chert petrology: *Geological Society of America Bulletin*, v. 117, p. 835–845, <https://doi.org/10.1130/B25555.1>.
- März, C., Riedinger, N., Sena, C., and Kasten, S., 2018, Phosphorus dynamics around the sulphate-methane transition in continental margin sediments: Authigenic apatite and Fe(II) phosphates: *Marine Geology*, v. 404, p. 84–96, <https://doi.org/10.1016/j.margeo.2018.07.010>.
- Munson, T.J., 2016, Sedimentary characterisation of the Wilton package, greater McArthur Basin, Northern Territory: *Northern Territory Geological Survey Record* 2016-003, 151 p.
- Planavsky, N.J., McGoldrick, P., Scott, C.T., Li, C., Reinhard, C.T., Kelly, A.E., Chu, X., Bekker, A., Love, G.D., and Lyons, T.W., 2011, Widespread iron-rich conditions in the mid-Proterozoic ocean: *Nature*, v. 477, p. 448–451, <https://doi.org/10.1038/nature10327>.
- Postma, D., 1981, Formation of siderite and vivianite and the pore-water composition of a recent bog sediment in Denmark: *Chemical Geology*, v. 31, p. 225–244, [https://doi.org/10.1016/0009-2541\(80\)90088-1](https://doi.org/10.1016/0009-2541(80)90088-1).
- Poulton, S.W., 2017, Biogeochemistry: Early phosphorus redigested: *Nature Geoscience*, v. 10, p. 75–76, <https://doi.org/10.1038/ngeo2884>.
- Pufahl, P.K., Anderson, S.L., and Hiatt, E.E., 2014, Dynamic sedimentation of Paleoproterozoic continental margin iron formation, Labrador Trough, Canada: Paleoenvironments and sequence stratigraphy: *Sedimentary Geology*, v. 309, p. 48–65, <https://doi.org/10.1016/j.sedgeo.2014.05.006>.
- Reinhard, C.T., Planavsky, N.J., Gill, B.C., Ozaki, K., Robbins, L.J., Lyons, T.W., Fischer, W.W., Wang, C., Cole, D.B., and Konhauser, K.O., 2017, Evolution of the global phosphorus cycle: *Nature*, v. 541, p. 386–389, <https://doi.org/10.1038/nature20772>.
- Rothe, M., Kleeberg, A., and Hupfer, M., 2016, The occurrence, identification and environmental relevance of vivianite in waterlogged soils and aquatic sediments: *Earth-Science Reviews*, v. 158, p. 51–64, <https://doi.org/10.1016/j.earscirev.2016.04.008>.
- Ruttenberg, K.C., and Berner, R.A., 1993, Authigenic apatite formation and burial in sediments from non-upwelling, continental margin environments: *Geochimica et Cosmochimica Acta*, v. 57, p. 991–1007, [https://doi.org/10.1016/0016-7037\(93\)90035-U](https://doi.org/10.1016/0016-7037(93)90035-U).
- Sánchez-Baracaldo, P., Ridgwell, A., and Raven, J.A., 2014, A neoproterozoic transition in the marine nitrogen cycle: *Current Biology*, v. 24, p. 652–657, <https://doi.org/10.1016/j.cub.2014.01.041>.
- Sperling, E.A., Wolock, C.J., Morgan, A.S., Gill, B.C., Kunzmann, M., Halverson, G.P., Macdonald, F.A., Knoll, A.H., and Johnston, D.T., 2015, Statistical analysis of iron geochemical data suggests limited late Proterozoic oxygenation: *Nature*, v. 523, p. 451–454, <https://doi.org/10.1038/nature14589>.
- Todd, S.E., Pufahl, P.K., Murphy, J.B., and Taylor, K.G., 2018, Sedimentology and oceanography of early Ordovician ironstone, Bell Island, Newfoundland: Ferruginous seawater and upwelling in the Rheic Ocean: *Sedimentary Geology*, v. 379, p. 1–15, <https://doi.org/10.1016/j.sedgeo.2018.10.007>.
- Tosca, N.J., Guggenheim, S., and Pufahl, P.K., 2016, An authigenic origin for Precambrian greenalite: Implications for iron formation and the chemistry of ancient seawater: *Geological Society of America Bulletin*, v. 128, p. 511–530, <https://doi.org/10.1130/B31339.1>.
- Tung, M.S., Eidelman, N., Sieck, B., and Brown, W.E., 1988, Octacalcium phosphate solubility product from 4 to 37 °C: *Journal of Research of the National Bureau of Standards*, v. 93, p. 613–624, <https://doi.org/10.6028/jres.093.153>.
- Van Cappellen, P., and Berner, R.A., 1991, Fluorapatite crystal growth from modified seawater solutions: *Geochimica et Cosmochimica Acta*, v. 55, p. 1219–1234, [https://doi.org/10.1016/0016-7037\(91\)90302-L](https://doi.org/10.1016/0016-7037(91)90302-L).
- Yang, B., Smith, T.M., Collins, A.S., Munson, T.J., Schoemaker, B., Nicholls, D., Cox, G., Farkas, J., and Glorie, S., 2018, Spatial and temporal variation in detrital zircon age provenance of the hydrocarbon-bearing upper Roper Group, Beetaloo Sub-basin, Northern Territory, Australia: *Precambrian Research*, v. 304, p. 140–155, <https://doi.org/10.1016/j.precamres.2017.10.025>.
- Zegeye, A., et al., 2012, Green rust formation controls nutrient availability in a ferruginous water column: *Geology*, v. 40, p. 599–602, <https://doi.org/10.1130/G32959.1>.

Printed in USA